Research article

Ahmed El-Mowafy* and Congwei Hu

Validation of BeiDou Observations

Abstract: This study presents validation of BeiDou measurements in un-differenced standalone mode and experimental results of its application for real data. A reparameterized form of the unknowns in a geometry-free observation model was used. Observations from each satellite are independently screened using a local modeling approach. Main advantages include that there is no need for computation of inter-system biases and no satellite navigation information are needed.

Validation of the triple-frequency BeiDou data was performed in static and kinematic modes, the former at two continuously operating reference stations in Australia using data that span two consecutive days and the later in a walking mode for three hours. The use of the validation method parameters for numerical and graphical diagnostics of the multi-frequency BeiDou observations are discussed. The precision of the system's observations was estimated using an empirical method that utilizes the characteristics of the validation statistics. The capability of the proposed method is demonstrated in detection and identification of artificial errors inserted in the static BeiDou data and when implemented in a single point positioning processing of the kinematic test.

Keywords: BeiDou, GNSS, Observation Precision, System Errors, Data Validation

***Corresponding Author: Ahmed El-Mowafy:** Department of Spatial Sciences, Curtin University Perth, WA, Australia, E-mail: A.El-mowafy@curtin.edu.au

Congwei Hu: Department of Surveying and Geo-informatics Tongji University, Shanghai

1 Introduction

In 2007, China started its own Global Navigation Satellite System - BeiDou (previously known as COMPASS) - by launching the first validation medium earth orbit satellite C30 (MEO - M1) [10, 13]. Currently (2014), the system includes four MEO satellites, five inclined geosynchronous orbit (IGSO) satellites, and five geostationary (GEO) satellites with an initial operational capability for a regional service over Asia-Oceania. [20] showed that in the Asia-Oceania area the average number of visible BeiDou satellites can be more than 16 (assuming a complete constellation), which would give average PDOP values less than 1.4. Over North America, the GEO and IGSO satellites are not visible in general and the average number of visible satellites would be about eight and the PDOP value would be more than 2.2.

In this contribution, data from BeiDou in all of its available frequencies are screened to detect and identify possible outliers in the data. BeiDou currently broadcasts signals in three frequencies, B1 at 1561.098 MHz, B2 at 1207.14 MHz, and B3 at 1268.52 MHz [15]. BeiDou will also broadcast a fourth frequency tentatively at 1589.74 MHz [12], but it is not utilized yet. BeiDou signal structure, codes, and strength were discussed in [2] and [11] for understanding the system interoperability and integration with GPS, Galileo and GLONASS. In each frequency band of BeiDou, two coherent sub-signals have been detected. These signal components are referred to In-phase "I" and quadrature "Q" [17]. The "I" components have shorter codes and are likely to be intended for the open service. The "Q" components have much longer codes, are more interference resistive, and are probably intended for the restricted service [14]. BeiDou signals have somewhat greater power than other GNSS.

Positioning using BeiDou requires a pre-processing quality control step for data screening to detect the most severe irregularities in the data and identify faulty observations. A geometry-free single-receiver single-satellite method can be used for this purpose. The method is presented in [5] and [7] for use in any GNSS constellation. In this contribution, its application for validation of BeiDou code and phase measurements on all of its three frequencies is discussed. In addition, the use of method statistics will be shown for estimation of BeiDou observation precision. The advantages of this approach for validation of BeiDou observations is that there is no need for computation of the inter-system biases as BeiDou measurements are validated without being integrated with other GNSS. Due to flexibility of the method, it can be applied under static or kinematic modes and quality control is applied for each satellite independently; thus, it allows one to present the necessary numerical and graphical statistical diagnostics for each satellite specific data quality.

The rest of the paper is organized as follows. Validation of GNSS observations using the single-receiver single-satellite approach is firstly briefly overviewed. The fol-

lowing sections discuss testing of the method for BeiDou, where diagnostics and estimation of signal stochastic properties from GEO, IGSO and MEO satellites are presented. Finally, evaluation of the method performance in the detection and identification of outliers in a test data are summarized and analyzed and practical application of the method in the kinematic mode is presented.

2 Validation of BeiDou observations

In this section, the single-receiver single-satellite method that will be used in this study for validation of BeiDou observations is briefly presented. The carrier phase and pseudorange observation equations of a single receiver for a single satellite on frequency f_i (for $i = 1, \ldots, n$, where i refers to the frequency identifier) at time instant k can be written as [4, 9, 16]:

$$\varphi_{ik} = \rho_k + d\rho_k + c(dt_r - dt_s) + T_k - \mu_i Ik + b_{\varphi_{ik}} + \delta_{\varphi_{ik}} + \varepsilon_{\varphi_{ik}} \quad (1)$$

$$p_{ik} = \rho_k + d\rho_k + c(dt_r - dt^s) + T_k + \mu_i I_k + b_{p_{ik}} + \delta_{p_{ik}} + \varepsilon_{p_{ik}} \quad (2)$$

where φ_{ik} and p_{ik} denote the observed carrier phase and pseudorange code measurements; respectively, with corresponding zero-mean random noise terms $\varepsilon_{\varphi_{ik}}$ and $\varepsilon_{p_{ik}}$. ρ_k is the receiver-to-satellite range, $d\rho_k$ is the orbital error, c denotes the speed of light, dt_r and dt^s are the receiver and satellite clock errors, and T_k is the troposphere delay. The parameter I denotes the ionosphere error expressed in distance units with respect to the first frequency, such that for frequency i, the ionosphere coefficient $\mu_i = \frac{f_1^2}{f_i^2}$ is applied. The parameters $b_{\varphi_{ik}}$ and $b_{p_{ik}}$ are the phase bias and the instrumental code delay. The phase bias is the sum of the initial phase, the phase ambiguity and the instrumental phase delay. $\delta_{\varphi_{ik}}$ and $\delta_{p_{ik}}$ denote the non-constant (or quasi-random) biases, e.g. multipath.

The model given in Eq. (1 & 2) shows that the problem at hand is underdetermined. One way to reduce the rank deficiency is to re-parameterize the unknowns in the observation equations as follows [5, 7]:

$$\rho_k^\star = \rho_k + d\rho_k + c(dt_r - dt^s) + T_k \quad (3)$$

$$\rho_k^{\star\star} = \rho_k^\star - \rho_{k_o}^\star \quad (4)$$

$$I_k^\star = I_k - I_{k_o} \quad (5)$$

$$b_{\varphi_{ik}}^\star = b_{\varphi_{ik}} + [\rho_{k_o}^\star - \mu_i I_{k_o}] \quad (6)$$

$$b_{p_{ik}}^\star = b_{p_{ik}} + [\rho_{ko}^\star + \mu_i I_{k_o}] \quad (7)$$

where k_o refers to the initial epoch of data processing. The observation equations hence read:

$$\varphi_{ik} = \rho^{\star\star} - \mu_i I_k^\star + b_{\varphi_{ik}} + \delta_{\varphi_{ik}} + \varepsilon_{ik} \quad (8)$$

$$p_{ik} = \rho_k^{\star\star} - \mu_i I_k^\star + b_{p_{ik}}^\star + \delta_{p_{ik}} + \varepsilon_{p_{ik}} \quad (9)$$

At the initial epoch k_o, the estimated non-constant biases are assumed zero, as their actual values are merged with the constant biases. $\rho_{k_o}^{\star\star}$ and $I_{k_o}^\star$ are zeros. Thus, $b_{\varphi_{ik}}^\star$ and $b_{p_{ik}}^\star$ are directly estimated from the measurements at k_o, and for a short period they can be treated as constants. The problem can be solved by using Kalman filtering. For dynamic modelling, the range term is assumed unlinked in time and the ionosphere and the non-constant biases, $\delta_{\varphi_{ik}}$ and $\delta_{p_{ik}}$, can be assumed changing relatively smoothly with time and modelled using a first order Gauss-Markov process.

The multi-frequency single-receiver single-satellite un-differenced GNSS observations vector (y_t), which in our case comprises BeiDou three-frequencies pseudorange code and phase observations, can be formulated in terms of the predicted state vector ($\check{x}$) of the unknowns $[\rho_k^{\star\star}, I_k^\star, b_{\varphi_{ik}}^\star, b_{p_{ik}}^\star, \delta_{\varphi_{ik}}, \delta_{p_{ik}}]^T$ in the linearized form:

$$y_k = A_k \check{x}_k + \hat{v}_k \quad (10)$$

with A_k denotes the design matrix, which reads:

$$A_k = \begin{bmatrix} u & -\mu_i & I & 0 & I & 0 \\ u^\star & +\mu_i & 0 & I & 0 & I \end{bmatrix} \quad (11)$$

where $i = 1$ to 3 frequencies for BeiDou (B1, B2 and B3), u is a unit column vector comprising three-elements, and I is a 3×3 identity matrix. $\hat{v}_k$ denotes the vector of observation predicted residuals and $Q_{\hat{v}_k}$ is their covariance matrix, where:

$$Q_{\hat{v}_k} = Q_{y_k} + [A_k \left(A_k Q_{y_k}^{-1} A_k \right)^{-1} \quad (12)$$

and Q_{y_k} is the covariance matrix of the observations.

Possible detection of the presence of model errors can be performed by examining the local over-all model statistic T_{LOM}, which can be formulated as [18]:

$$T_{LOM} = \hat{v}_k^T Q_{\hat{v}_k}^{-1} \hat{v}_k / df \quad (13)$$

This statistic has a Fisher distribution under a null hypothesis of an outlier-free case. Therefore, one may assume possible presence of measurement or model errors when:

$$T_{LOM} \geq F_a(df, \infty, 0) \quad (14)$$

where F_α is a critical value of Fisher distribution computed for a pre-set significance level (α) and df, where df is the degrees of freedom for m observations. If the detection test passes, then testing stops at the current epoch and the same procedure is applied in the next epoch. If the test fails, identification of possible observations that may carry the errors should be performed. We will restrict attention here to outlier identification in testing single observations, and the test static w_j for observation j can be given as [18]:

$$w_j = \frac{c_j^T Q_v^{-1} \hat{v}}{\sqrt{c_j^T Q_v^{-1} c_j}} \tag{15}$$

where c_j is a zero column vector except the element corresponding to the examined observation, which equals 1. The w_j statistic has a standard normal distribution under the null hypothesis. Thus, an outlier is suspected to be present in the observation j when:

$$\begin{aligned} |w_j| &\geq \left\{ N_{\frac{\alpha}{2}}(0,1) \right\} \\ |w_j| &> |w_1| \ \forall q = 1, \ldots, m \end{aligned} \tag{16}$$

where m is the number of observations, $\left\{ N_{\frac{\alpha}{2}}(0,1) \right\}$ denote standard normal distribution for a significance level α' for $w-$statistic

3 Test Description for Validation of BeiDou Measurements

In this study, validation of BeiDou measurements is investigated in un-differenced standalone mode where data from each satellite are independently processed using the presented single-receiver single-satellite approach in static and kinematic modes. The static data used for testing were collected at two CORSs at Curtin University, Perth, Western Australia. The test site can track most available BeiDou satellites in its current constellation. The data span two consecutive days as a representative sample, i.e. 1/3/2014 and 2/3/2014, with 30 seconds sampling interval. Tracked signals in the test included BeiDou B1, B2 and B3 code and carrier-phase observations of the "I" component.

The static data were collected using geodetic-grade multi-frequency multi-constellation antennae (TRM59800.00) and two receivers (Trimble NetR9), denoted as CUT0 and CUTa. The former is a station contributing in the current Multi-GNSS Experiment (MGEX) of the International GNSS Service (IGS) and is frequently used by researchers across the world for testing multi-constellation GNSS signals. The two receivers at CUT0 and CUTa are located at a distance of 8.418 m. Data from each receiver were processed independently and their results were compared to indicate possible receiver errors if differences are found. In addition, another test was performed in a kinematic walking mode using Trimble R10 receiver at Curtin University campus on 25/9/2013, where almost three hours of data of one-second sampling interval were collected. In general, eight to eleven BeiDou satellites were observed during the kinematic test period except for a few epochs, where only four satellites were observed due to passing close to tree canopy.

The following sections present results of monitoring and analysis of the data validation parameters for the two test modes. Due to the large number of the resulting related figures, only a representative sample of the figures will be given for each case. Moreover, characterization of the stochastic properties of the signals and evaluation of the method performance will be discussed.

4 Monitoring and Analysis of Data Validation Parameters

For detection of errors, the TLOM values were computed at each epoch and for each satellite. Figure 1 shows an example of the time series of T_{LOM} and its histogram for C1 (GEO satellite) at station CUT0 computed on 1/3/2014 and the test threshold (Fisher distribution critical value) defined as K_{LOM}, which is shown as a solid line. Note here that the number of observations at each epoch was identical during the test (one code and one phase for the three frequencies), which gave a constant value of df. The C1 GEO satellite has an elevation angle of approximately 43° from the test site at Curtin University. An error can be suspected if T_{LOM} exceeds the threshold as depicted at a few epochs in the figure.

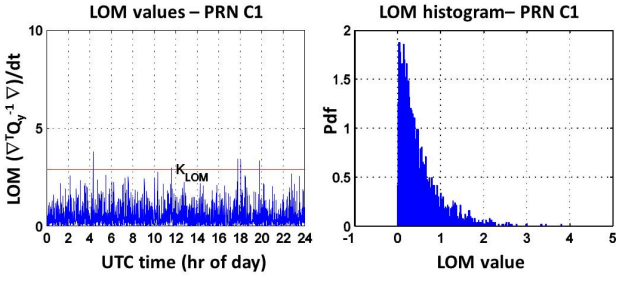

Fig. 1. T_{LOM} static for PRN C1 at station CUT0.

For identification of the observations that have errors at epochs where the detection test fails, the w-statistic was computed using Eq. (15). Figure 2 shows on its left side time-series of the computed w-statistic for C1 at CUT0, for the phase data ϕ(B1, B3, B2 frequencies) and the code observations p(B1, B3 and B2), respectively. The w-statistic critical values are shown as solid lines. The signal-to-noise ratio (SNR) in dB-Hz for B1 is illustrated at the bottom of the left side of the Figure 2 along with the elevation angle. Similar performance was observed when processing the data of CUTa as illustrated in Figure 3. Thus, no errors were identified due to receiver hardware specific outliers.

The critical (thresholds) values for the w–statistic $\left\{N_{\frac{\alpha}{2}}(0,1)\right\}$ are shown as solid red lines in the figures. A possible outlier is suspected when the computed w-statistic exceeds this critical value. In practice, the significance level (α') needed for the computation of the critical values should be selected based on requirements of the application at hand. It is assumed here that α' for the w-test equals 0.001, which is a reasonable assumption for precise applications. For detection testing, a different value of the significance level (α) should be used. This α can be computed using Baarda's B method [1], which assumes same probability for type II error (failure to reject a false null hypothesis) in both the detection and identification tests. In this study, this probability is taken equals 0.2, which is a typical value used for this type of testing.

The distribution of the w–statistic can give a good diagnostics of the correctness of the model used as this distribution should follow a standard normal distribution. The right side of the Figure 2 and Figure 3 illustrate the histograms of the corresponding w-statistics and their computed standard deviation (ρ_w) and mean (μ_w), which are given on top of each histogram plot. Visual inspection of the histograms reveals that the w–statistic varies in a random manner with a standard normal distribution and the computed ρ_w and μ_w were close to 1 and 0 (with some discrepancies due to noise in the data). In addition, one may inspect the Q-Q plot of the w–statistic where a departure from its slant straight line would indicate departures from normality. Figure 4 and Figure 5 give two examples of the Q-Q plots for the B1 signal for the static and kinematic tests for C1 satellite. Overall, these figures indicate appropriateness of the model used as wrong model would lead to a wrong distribution of the w–statistic.

The previous figures show w–statistic values for C1 as an example of GEO satellites. Figure 6 and Figure 7 show two examples of the other types of BeiDou satellites, the IGSO and MEO satellites, represented by the satellites C8 and C13, respectively as observed at CUT0 on 1/3/2014. The gap shown in the data in Figure 7 between the hours 5:50 and 9:15 UTC is due to unavailability of satellite signals.

In GNSS, the signals are precisely controlled by the atomic clocks as these clocks produce the reference for the signals [9]. Therefore, although the presented method is insensitive to clock errors as they are absorbed in the term (ρ_k^{**}) in Eq. (3-4), and thus will not affect T_{LOM} or w–statistic, instability of the clocks will show up due to disturbance in the observations and their predicted values computed through the dynamic model. The clock of satellite PRN C30, the first-launched MEO satellite (known as M1), was reported earlier by [8] to experience some problems. This was confirmed by our data analysis. For example, Figure 8 displays the w-statistic for code data on B1 and B2 (denoted as p2 and p5b) of M1 collected on February 22, 2012. As the figure shows, there were multiple errors detected during this period, which had resulted in a distribution of the w-statistics not in agreement with the theoretical standard normal distribution as can also be shown from its skewed distribution in the Q-Q plot depicted in Figure 9.

5 Characterization of the Stochastic Properties of the Signals

The TLOM and w–statistic results presented in this study using the single-receiver single-satellite method were computed assuming no auto-correlation or cross-correlation among code and phase measurements in the stochastic model, and thus, the covariance matrix of the undifferenced measurements was a diagonal matrix. Rigorous values of the precision of undifferenced BeiDou satellite signals are still under investigation by several researchers [3]. In this study, the zenith-referenced values of standard deviations of BeiDou phase and code observations were empirically estimated using a curve fitting iterative approach.

The static data used for this purpose were collected over three days between 25/2/2014 and 27/2/2014. In this process, different possible values of standard deviations were iteratively used in the validation task, and the set that gives the best overall fit of the distribution of w-statistic to $N(0, 1)$ for most satellite observations was selected as the best candidate. For phase observations, their standard deviations were iterated within the range 0.5 mm to 3 mm, and using increments of 0.1 mm between successive iterations. Standard deviations of code observations were examined between 5 cm and 30 cm, with increments of

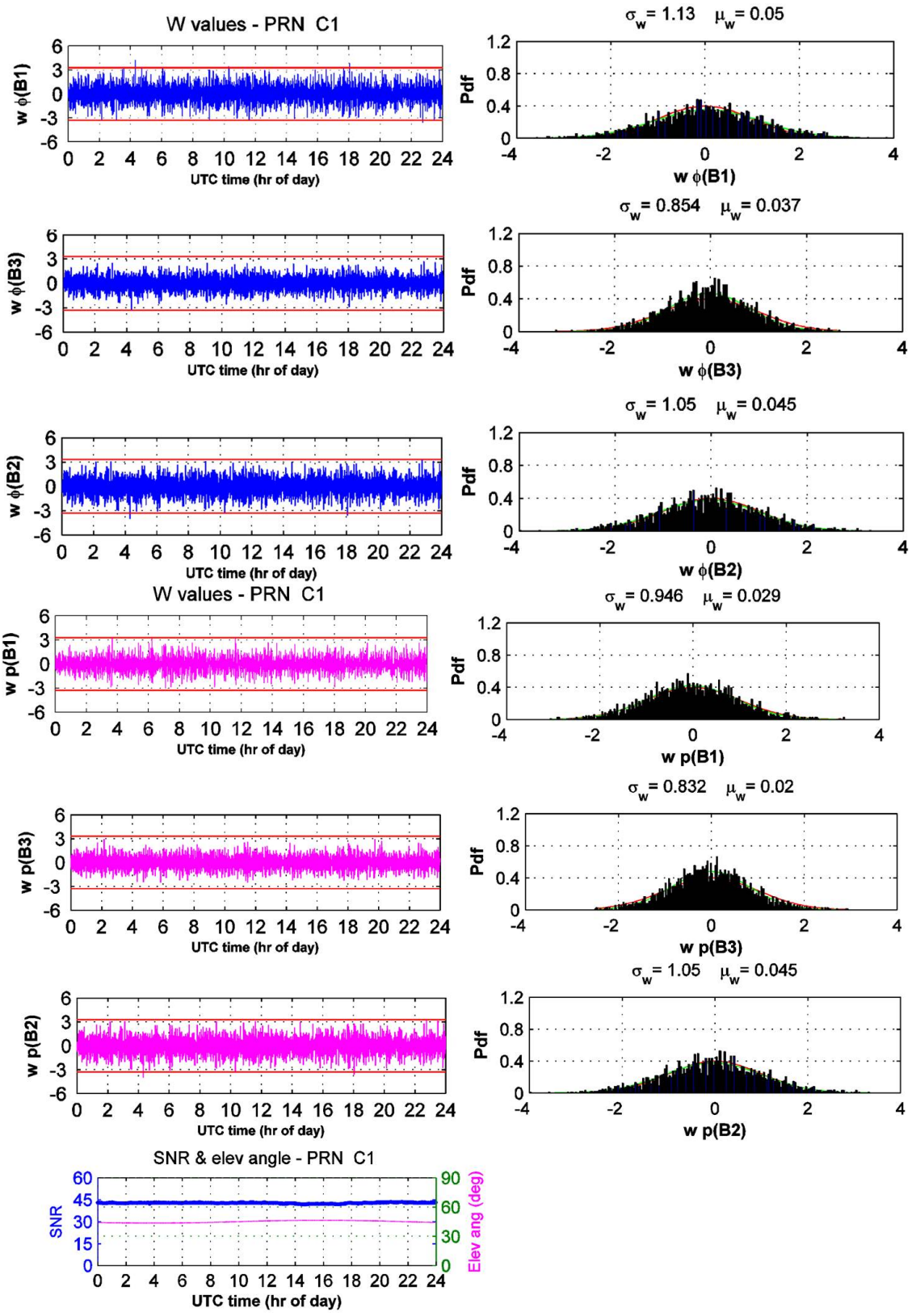

Fig. 2. *w*–test static for PRN C1 at station CUT0, left side shows time series of w-statistic for the code and phase observations and SNR values, right side shows histogram of the w-statistic.

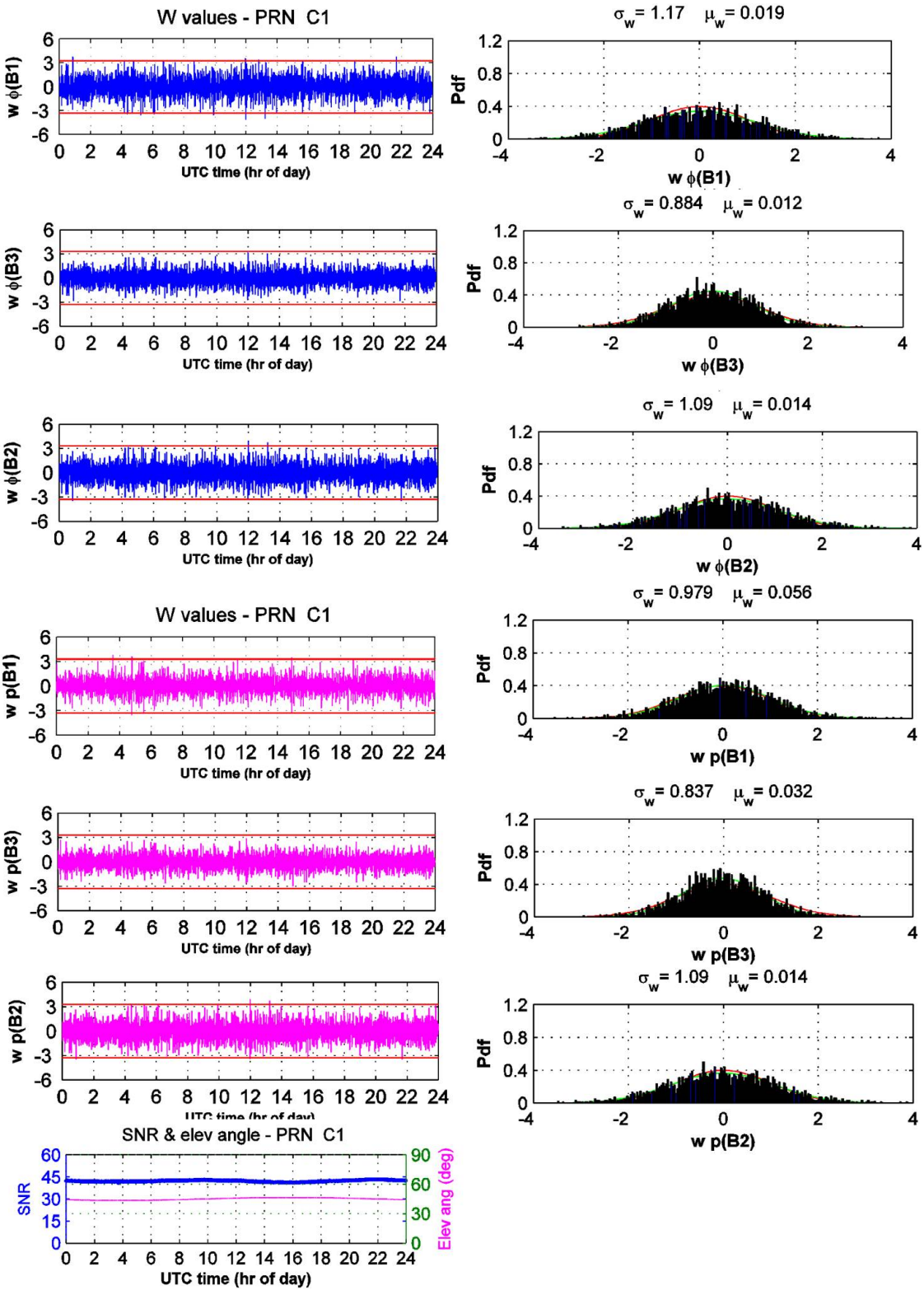

Fig. 3. *w*–test static for PRN C1 at station CUTa.

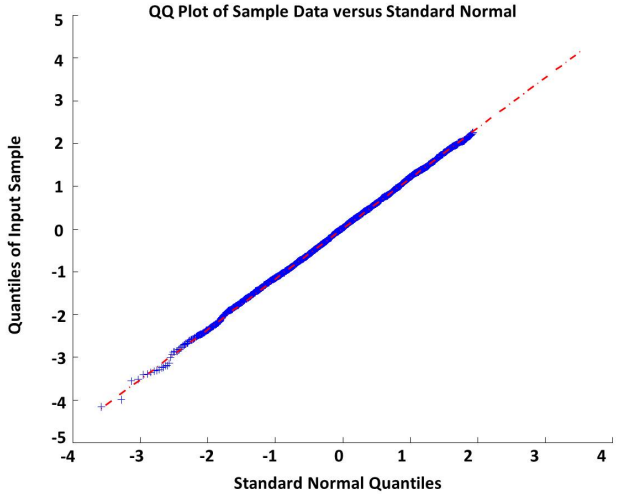

Fig. 4. Q-Q plot of B1 w-statistic for PRN C1 in the static test at CUTa.

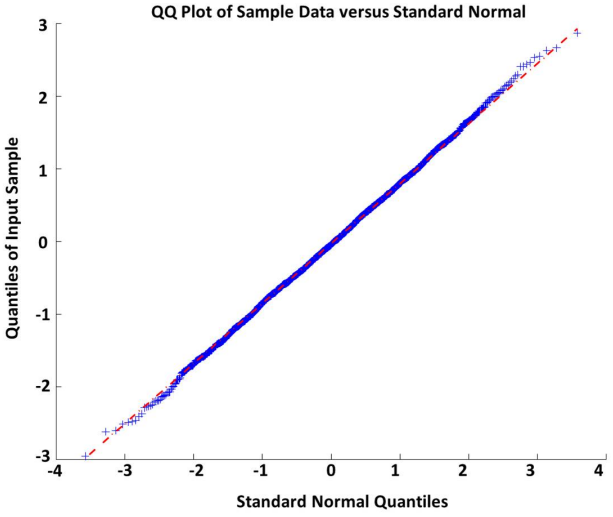

Fig. 5. Q-Q plot of B1 w-statistic for PRN C1 in the kinematic test.

1 cm. The best set of zenith standard deviations resulting from this study are given in Table 1. It is important to note that the impact of multipath is not included in these values, as multipath was modelled out through estimation of $\delta_{\varphi_{ik}}$ and $\delta_{p_{ik}}$. Multipath is a significant error source in particular for the GEO satellites. The standard deviations for the slant observations along the receiver-to-satellite line of sight (ρ) can be computed using the observed elevation-angle, utilizing for instance an elevation-angle dependent model [6].

The standard deviations for the slant observations can also be computed as a function of the Carrier-to-Noise density ratio (or the signal-to-noise ratio, SNR), such that for observation j [19]:

$$\sigma_j^2 = Z_j \times 10^{-\frac{SNR_i}{10}} \tag{17}$$

where Z_j is a variance factor that is dependent on the type and frequency of the observation, the method used for signal tracking and receiver used. SNR_j is the measured SNR for observation j in dB-Hz. In this research, the Z_j variance factor for BeiDou was estimated along the zenith by substituting for the observation variance in the left side of Eq. (17) with the values given in Table 1, and using the maximum values of SNR, which are usually reached close to zenith. It is worth noting here that BeiDou signals have high carrier-to-noise density ratios, which exceed the values for the signals of other constellations such as GPS and Galileo on the corresponding frequency bands [8]. In our test, SNR of BeiDou signals reached a maximum of 56 dB-Hz.

Table 1. Standard deviation of undifferenced BeiDou measurements.

	B1	B2	B3
code (cm)	8	8	8
phase (mm)	1.5	2	1.5

Stochastic information needed for processing using the single-receiver single-satellite validation method include the precision of the process noise of the ionosphere and non-constant biases and their correlation times. These unknowns are modelled as a first-order Gauss-Markov process with a correlation that is decaying exponentially with time. Therefore, their correlation times were determined by estimating the time lag at which the autocorrelation equals $1/e$ (where e refers to the base of the natural logarithm). In this research, the variances of the process noise were estimated using the same approach used for estimating the precision of the observations, i.e. selecting the set that gives the best overall fit of the distribution of w–statistic values to $N(0, 1)$. Table 2 gives the values of correlation time and process noise standard deviations estimated from processing BeiDou static data over the period 25/2/2014 to 27/2/2014, and Table 3 gives the corresponding values for the kinematic test. As seen from the comparison between the two tables, there were very little discrepancies between the values of the parameters under consideration, bearing in mind the low dynamic experienced in the kinematic test, where the discrepancies were only limited to the standard deviations of the non-constant biases.

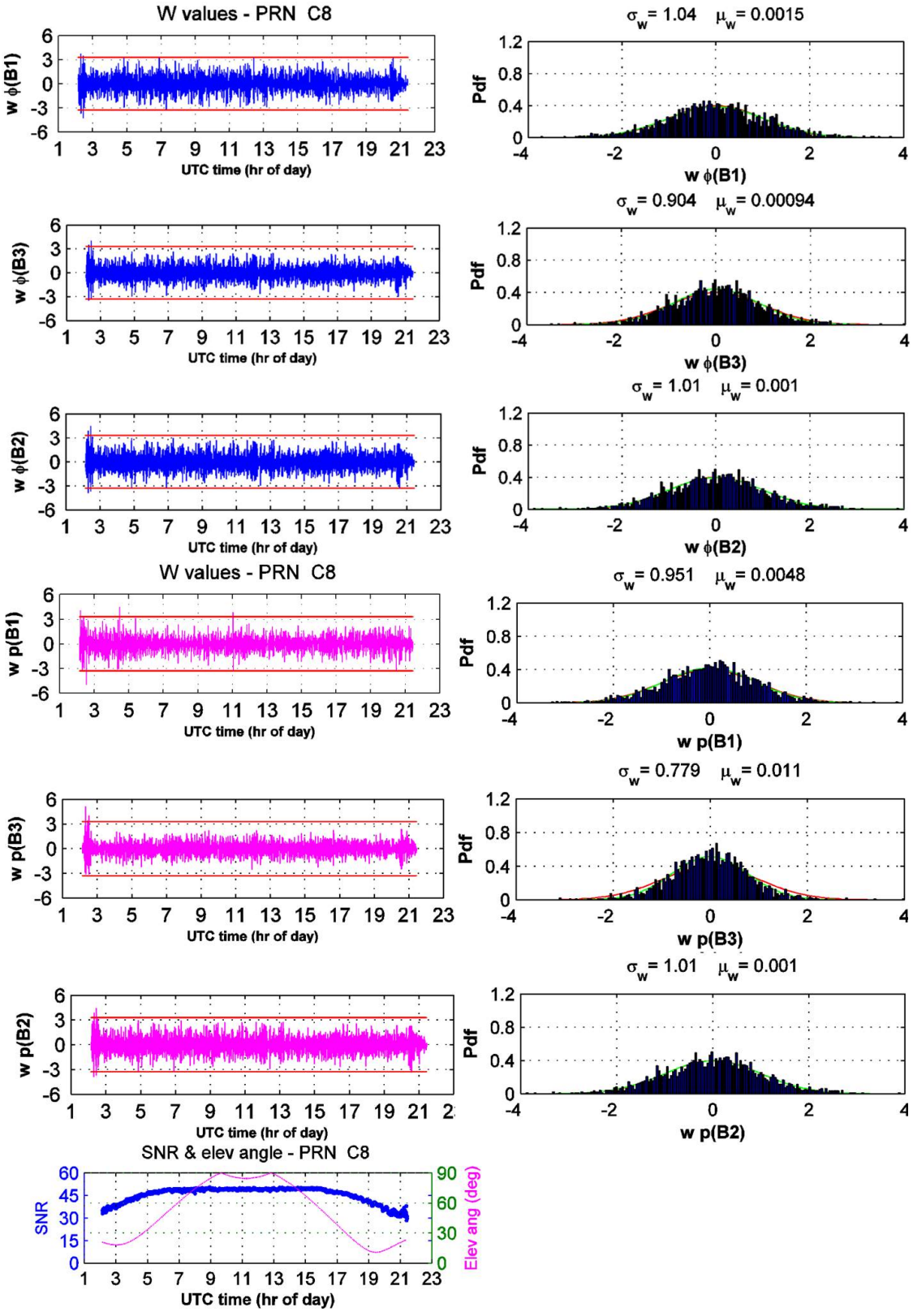

Fig. 6. *w*–test static for PRN C8 (IGSO) at station CUT0.

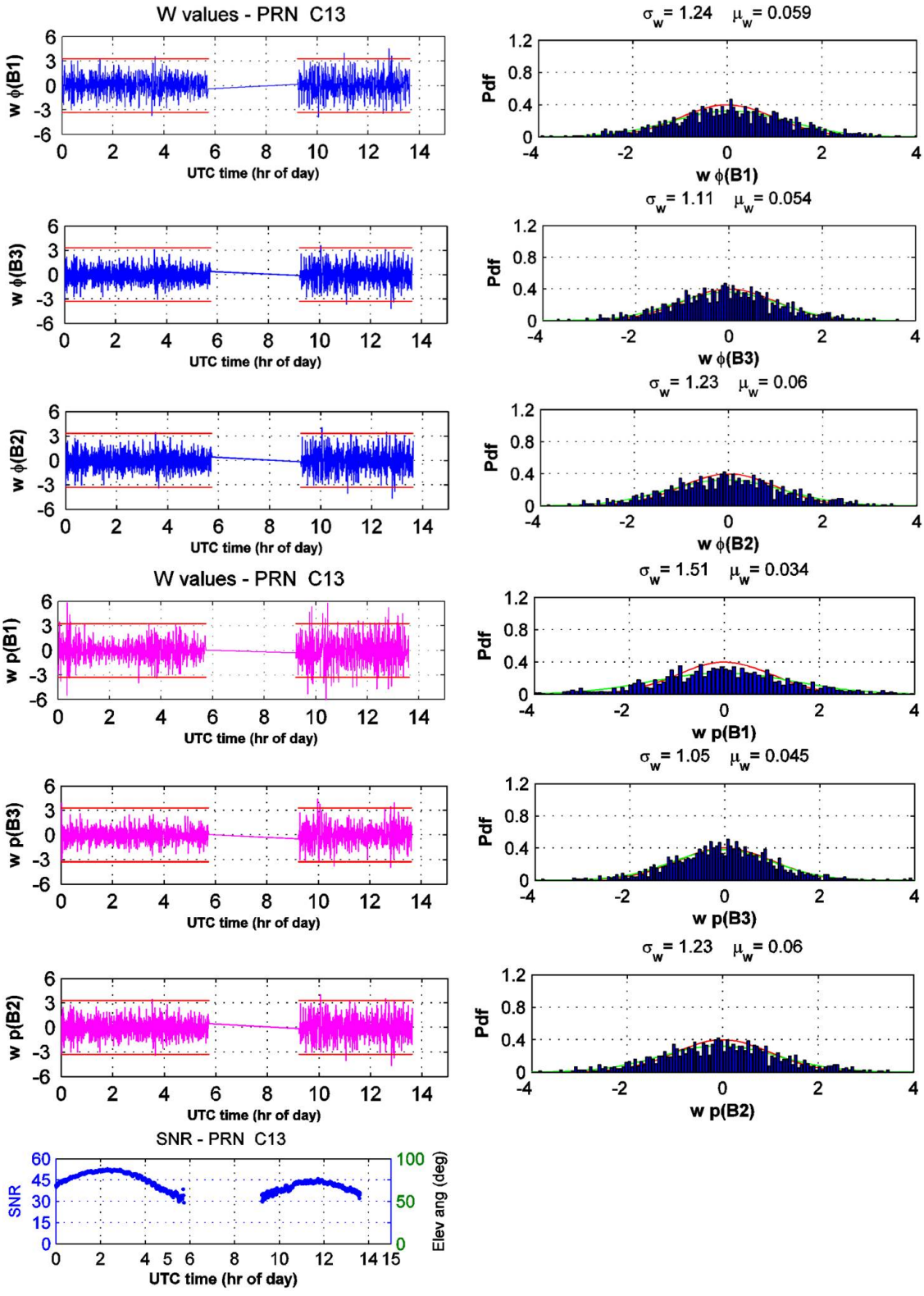

Fig. 7. *w*–test static for PRN C13 (MEO) at station CUT0.

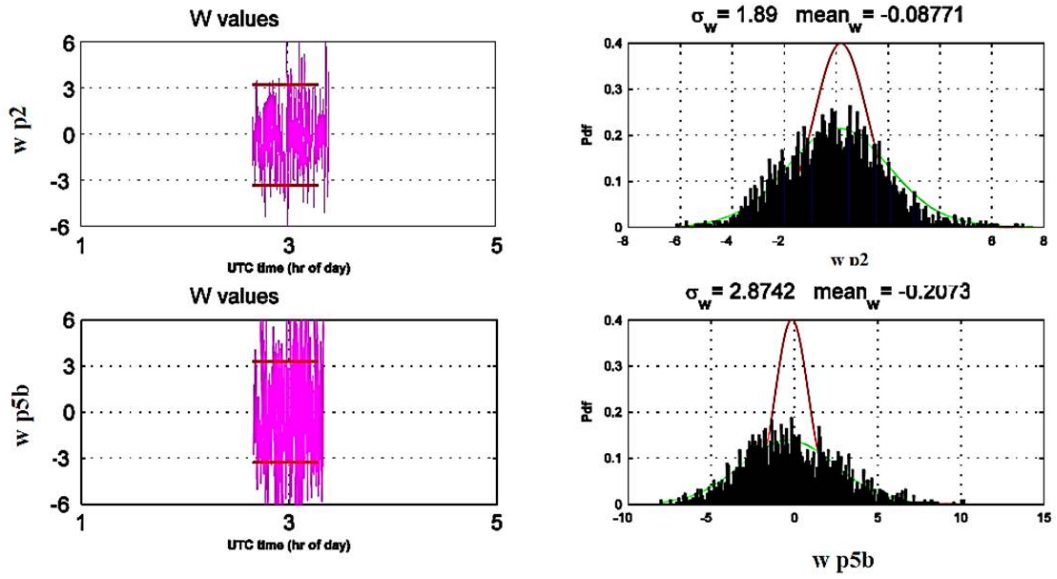

Fig. 8. *w*–test static for PRN C30-M1 during clock instability period.

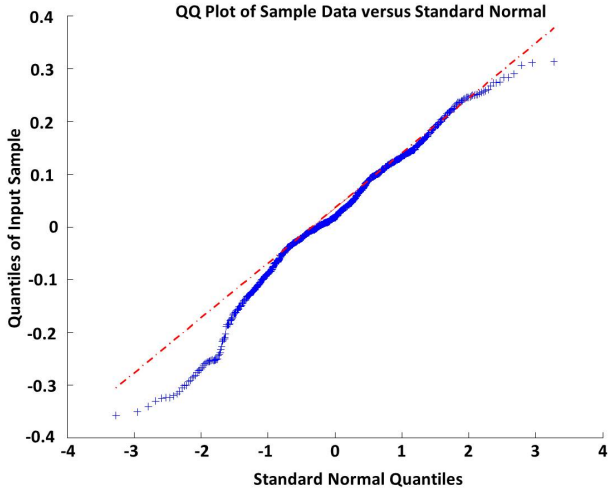

Fig. 9. Q-Q plot of w-statistic for PRN M1 during clock instability period.

Table 2. Dynamic modeling parameters (static mode).

	Standard deviation of process noise (cm)	Correlation time (sec)
ionosphere	2.00	600
non-constant phase bias	0.23	900
non-constant code bias	5.30	900

Table 3. Dynamic modeling parameters (kinematic mode).

	Standard deviation of process noise (cm)	Correlation time (sec)
ionosphere	2.10	600
non-constant phase bias	0.20	900
non-constant code bias	5.00	900

6 Evaluation of Method Performance in Detection and Identification of Errors in BeiDou Observations

To evaluate performance of the proposed algorithm for detection and identification of observation outliers of BeiDou observations, the following approach was carried out. First, several artificial errors were inserted at known epochs in the static test data collected on 1/3/2014 and 2/3/2014 with 30 seconds sampling interval. Next, the proposed single-receiver single-satellite validation approach was performed in the local mode. After its processing, a check was performed to examine whether the algorithm was able to detect and identify the presence of the inserted errors at their known epochs. A total of 644 artificial errors were inserted in the static data. These errors were of

random values but bounded within a specific range. For phase errors, the inserted errors ranged from 1 cycle to 9 cycles. For code observations, the minimum inserted error was 1.5 m and the maximum error was 7.5 m. These ranges were selected such that the minimum values are close to the minimal detectable biases (MDB), which is the minimum error that can be detected for each observation type with the chosen probabilities of false alarm and missdetection, which were taken as 0.001 and 0.2 respectively. The errors were generated using the MATLAB code "rand". The inserted errors had almost a uniform distribution.

The inserted errors in phase and code observations were categorized into three bands, and the method success rates in detection of the errors in these bands were assessed. For phase data, the three bands include artificial outliers within the ranges 1 to 3 cycles, 3 to 6 cycles, and 6 to 9 cycles. The numbers of inserted errors in each of these bands were 108, 106, and 107, respectively. For code observations, the three assumed outlier groups were within the three ranges 1.5 m - 3.5 m, 3.5 m - 5.5 m, and 5.5 m - 7.5 m. The numbers of artificial outliers that were inserted in these three groups were 108, 107, and 108, respectively. The specific epochs and observations where these errors were inserted as well as their values were recorded for comparison with detection results obtained from the data validation method.

Table 4 and Table 5 summarize the number of detected outliers using the single-receiver single-satellite validation approach and their percentage with respect to the total number of the inserted errors in each category for phase and code observations. Over the two test days, the overall average of successful detection for phase errors that were between 1 cycle and 3 cycles was 88% and increased 92% for the range between 3 cycles and 6 cycles. The error detection success rate has reached almost 99% for errors that were between 6 cycles and 9 cycles. For code observations, the success rate in detection of the inserted code errors was in general similar to that of the phase errors, except for the range of 3.5 m to 5.5 m, where code outliers were detected at almost 99%. These results reflect the good performance of the proposed method for detection of errors of BeiDou observations.

For the epochs where detection was successful, checking is performed to examine if the observations that contain the artificial errors can be correctly identified by the identification test. Due to the high correlations among test statistics for phase observations, which were higher than 0.9 in general, identification was only performed for outliers in code observations, which had negligible correlations among their test statistics. Table 6 shows the overall percentage for identification of code outliers for the data where errors were detected. Results showed that the success rates of identification of outliers for the three error bands were above 90% and, as expected, increased as error size increased. The single-receiver single-satellite approach was successful in identifying 92%, 97%, and 100% of outliers in the three error bands: 1.5-3.5 m, 3.5-5.5 m, and 5.5-7.5 m, respectively. Future work is planned to apply the method in the 'global' mode, whereby data from more than one epoch are used in testing. This approach has a good potential to improve the detection and identification performance.

In a practical application of the method, the single-receiver single-satellite validation approach was implemented for the kinematic test data in a pre-processing step. The filtered BeiDou data were next processed unaided by any other GNSS constellation in a single point positioning (SPP) mode. The used receiver (Trimble R10) was running for the same test period in an RTK mode using GPS data. The positioning solution of the GPS RTK was used as the reference (assumed as ground truth) for comparison with the BeiDou SPP solution. The time-series of the differences

Table 4. Number of detected phase errors and their percentage.

1-3 cyc		3-6 cyc		6-9 cyc	
Inserted errors	detected errors	Inserted errors	detected errors	Inserted errors	detected errors
108	95	106	98	107	106
88%		92%		99 %	

Table 5. Number of detected code outliers and their percentage.

1.5-3.5 m		3.5 - 5.5 m		5.5 - 7.5 m	
Inserted errors	detected errors	Inserted errors	detected errors	Inserted errors	detected errors
108	97	108	107	107	107
90%		99%		100%	

Table 6. Identification of code outliers.

1.5-3.5 m		3.5 - 5.5 m		5.5 - 7.5 m	
Inserted errors	Identified errors	Inserted errors	Identified errors	Inserted errors	Identified errors
97	89	107	104	107	106
92%		97%		99%	

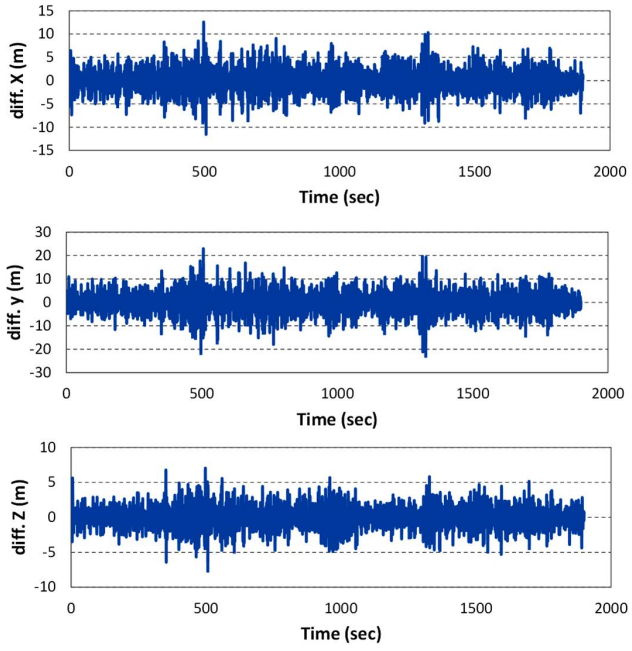

Fig. 10. BeiDou SPP position differences from GPS RTK.

between the two positioning solutions in WGS-84 X, Y, Z coordinates are given in Figure 10. As the figure shows the differences in X and Z coordinates were in general within ±5 m, whereas the Y differences were within ±10 m (mainly due to geographical location of the test, satellite geometry and mapping of errors along the Cartesian axes). The errors were larger at a few epochs, seen as small spikes in the figures, which is mainly attributed to observing a low number of satellites when passing close to tree canopies. In general, these limited results somewhat show the effectiveness of the single-receiver single-channel data validation method through the absence of unwanted observation irregularities in the processed data (which could be seen as large spikes in the figure) after implementation of the method in a pre-processing step.

7 Conclusion

Quality control of BeiDou GEO, IGSO and MEO satellite measurements is presented by screening data for severe irregularity using a single-receiver single-satellite local validation approach. The method is applicable to any GNSS with any arbitrary number of frequencies. Testing included BeiDou B1, B2 and B3 code and phase observations for several days of static data and in a kinematic test.

The paper demonstrates the use of the w-statistic as a diagnostics tool to check the correctness of the model used as the w-statistic should have a standard normal distribution. Precision of undifferenced phase and code BeiDou observations (excluding multipath effect) were empirically estimated using a curve fitting iterative approach. Possible values of the stochastic parameters for process noise and correlation time of the unknowns were estimated in the static and kinematic modes.

To evaluate the capability of the proposed algorithm for the detection of errors, 644 artificial errors were inserted in a static data set that spans two days. The inserted errors ranged from 1 cycle to 9 cycles for phase errors, and from 1.5 m to 7.5 m for code observations with almost a uniform distribution. The single-receiver single-satellite approach was successful in detecting 88% to 99% of the phase and code outliers according to the size of the outliers. Evaluation of the method performance in correct identification of the code observations that had the artificial outliers showed that the method success rate ranged between 92% and 99%. Effectiveness of the method is also demonstrated by comparing BeiDou only SPP solution in the kinematic mode, after being validated by the single-receiver single-satellite method, with GPS RTK solution where unusual differences between the two solutions were not seen.

Acknowledgments

The author would like to thank Prof. Peter Teunissen for his comments. This work was funded through an IRG grant from Curtin University of Technology, project number 47606. The GNSS Research Centre at Curtin University is acknowledged for providing the static test data.

References

[1] Baard W. A. A testing procedure for use in geodetic networks, Netherlands Geodetic Commission, Publications on Geodesy, New Series, 2(5), 1968.

[2] Cao C., Jing G., and Luo M., COMPASS satellite navigation system development. PNT challenges and opportunities symposium, Stanford, California, USA, 5–6 Nov 2008.

[3] Chen L., Zhao Q., Hu Z., Zhao Y. and Xiang F., Preliminary Analysis on Pseudorange Data Quality and Positioning Accuracy of Beidou Satellite Navigation System, *Proc. The 3rd China Satellite Navigation Conference (CSNC 2012)*, Guangzhou, China, Springer, 15–19 May, 2012, 21-30.

[4] El-Mowafy A., Decimeter Level Mapping Using Differential Phase Measurements of GPS Handheld Receivers, *Survey Review*

38(295) (2005), 47-57.
[5] El-Mowafy A., Teunissen P., and Odijk D., Single-Receiver Single-Channel Real-Time Validation of GPS, GLONASS, Galileo and COMPASS Data, *Proc. International Symposium on GPS/GNSS*, Taipei, Taiwan, 26-28 Oct., 2010.
[6] El-Mowafy, A., Analysis of the Web-Based Post-Processing GNSS Services for Static and Kinematic Positioning in Surveying Applications of Short Data Spans, *Survey Review* **43**(323) (2011), 535-549.
[7] El-Mowafy A., GNSS Multi-frequency Receiver Single-Satellite Measurement Validation Method, *GPS Solutions*, Published online, 2014, DOI 10.1007/s10291-013-0352-6.
[8] Hauschild A., Montenbruck O., Sleewaegen J. M., Huisman L., and Teunissen P. J. G., Characterization of Compass M-1 Signals, *GPS Solutions* **16**(1), 2012, 117-126.
[9] Hofmann-Wellenhof B., Lichteneger H., and Wasle E., *GNSS-Global Navigation Satellite Systems GPS, GLONASS, Galileo, and More*, 2008, Springer, Wien, NY.
[10] Gao G. X., Chan A., Lo S., De Lorenzo D., and Per Enge, GNSS Over China: The Compass MEO Satellite Codes, *Inside GNSS* **7**(8) (2007), 36-42.
[11] Gao G. X., Chan A., Lo S., De Lorenzo D., Walter T., and Per Enge, Compass-M1 Broadcast Codes and Their Application to Acquisition and Tracking, *Proc. ION_NTM 2008*, San Diego, California, 28-30 January, 2008, 1-9.
[12] Gao G. X., Chan A., Lo S., De Lorenzo D., Walter T., and Per Enge, Compass-M1 broadcast codes in E2, E5b, and E6 frequency bands, *IEEE J Selected Topics in Signal Processing* **3**(4) (2009), 599–612.
[13] Gibbons. G., China GNSS 101: Compass in the rear view mirror, *Inside GNSS* **8**(1) (2008), 62-63
[14] Grelier,T., Dantepal J., DeLatour A., Ghion A. and Ries L., Initial Observations and Analysis of Compass MEO Satellite Signals, *Inside GNSS* **5**(6) (2007), 39-43.
[15] Gurtner W., and Estey L., RINEX: The Receiver Independent Exchange Format Version 3.01, accessed online on Nov 2013: http://igscb.jpl.nasa.gov/igscb/data/format/rinex301
[16] Misra P., and Enge P., *Global Positioning System: Signals, Measurements, and Performance*, 2nd Edition, 2005, Ganga-Jamuna Press.
[17] Sleewaegen J. M., 360 degrees—Compass signal quirks, another Navi Forum, *Inside GNSS* **5**(4) (2010), 14–15.
[18] Teunissen, P. J. G., Kleusberg A., *GPS for Geodesy*, 2nd ed., 1998, Springer, NY.
[19] Ward, P., GPS Satellite Signal Characteristics, in *Understanding GPS Principles and Applications*, (ed. Kaplan, E.D.), Artech House Publishers, 1996, 83-117.
[20] Zhang S., Guo J., Li B., and Rizos C., An analysis of satellite visibility and relative positioning precision of COMPASS, *Proc. Symp. for Chinese Professionals in GPS*, Shanghai, P.R. China, 18-20 August, 2010, 41-46.

Received December 04, 2013; accepted April 14, 2014.